MACHINE BUILDING AND MACHINE SCIENCE
МАШИНОСТРОЕНИЕ И МАШИНОВЕДЕНИЕ

UDC 621.9:531.3
https://doi.org/10.23947/2687-1653-2026-26-1-2103

Original Theoretical Research

Vibration Control of Tool Flank Wear in Turning

Valery E. Gvindjiliya
Don State Technical University, Rostov-on-Don, Russian Federation
✉ vvgvindjiliya@donstu.ru

EDN: EYOAES

Abstract

Introduction. The wear rate of a cutting tool can be controlled by introducing additional vibrations into the cutting zone. The effect of vibration parameters on tool wear appears to be well-studied. However, the conclusions of some such studies are contradictory. It is noted that vibrations of varying amplitudes can both increase and decrease wear. There are no analytical models in the literature that resolve this contradiction or reflect the nonlinear relationship between the tool and workpiece subsystems under cutting. Furthermore, the fact that wear on different tool faces requires different force interaction models is not taken into account. The present research fills these gaps. The objective of the study is to determine the patterns of impact of high-frequency vibrations (HFV) on tool flank wear.

Materials and Methods. The data from mathematical modeling of the dynamic cutting system in Simulink were used, taking into account the forces on the back face, effective parameters, and the HFV. Equipment: 16K20 machine tool, vibration control measuring stand with a frequency range of 0.4–15000 Hz, computer, E20-10 analog-to-digital converter, acoustic system, and STD.201-1 cutting force testing stand. Workpieces made of 10GN2MFA steel with a diameter of D = 84 mm were machined using tools with brazed T15K6 plates without lubrication.

Results. The effect of the HFV on the contact interaction forces along the tool flank and the phase trajectory of the tool deformation displacements are demonstrated for different HFV amplitudes: from $0.5 \cdot 10^{-2}$ to $2 \cdot 10^{-2}$ mm. It is established that power N of irreversible energy transformations (IET) depends on the direction of the introduced vibrations. The dependence of tool wear rate on additional vibrations with amplitudes of 5 and 10 μm in different directions at cutting speeds of 1 m/s, 1.4 m/s, and 2 m/s is shown. The results obtained are compared with wear trajectories without disturbances.

Discussion. The optimal amplitude of additional vibrations in the feed direction depends on the tool clearance and decreases with wear stage. The maximum wear value drops from 0.55 mm to 0.35 mm when introducing vibrations with an amplitude of 5 μm and to 0.26 mm — at 10 μm. With additional vibrations in the tangential direction, wear rate depends weakly on the amplitude of the introduced vibrations, as it is many times smaller than the velocity of the tool vibrational displacements. The maximum wear value decreases from 0.65 mm to 0.6 mm at 5 μm and to 0.48 mm — at 10 μm. With increased wear, there is no optimal amplitude for additional vibrations.

Conclusion. The developed models allow for a quantitative assessment of the impact of HFV on the tool flank wear rate and the appropriate selection of vibration parameters introduced into the cutting zone. This allows for the creation of:
– virtual models of the cutting process and the selection of modes to minimize wear rate;
– wear monitoring systems with a comprehensive approach to prediction.
Next, it is required to study the dynamics of the cutting process at HFV amplitudes greater than 10–15 μm.

Keywords: high-frequency vibrations, additional vibrations, dynamic cutting system, tool wear, irreversible energy transformations

Acknowledgements. The author would like to thank Dr.Sci. (Engineering), Professor V.L. Zakovorotny for fruitful discussions and significant recommendations during the preparation of the material. In addition, the author appreciates the assistance of the staff of the laboratory of the Research Institute for Vibrotechnology, Don State Technical University, in conducting scientific experiments.

Funding Information. The work is done within the framework of the Agreement for the implementation of applied scientific research “Development of Software and Hardware for Monitoring and Analysis of Cutting Parameters and Operational Characteristics of CNC Machines” (FZNE–2025–0008) no. 075–03–2025–302/10 dated 23.12.2025.

For Citation. Gvindjiliya VE. Vibration Control of Tool Flank Wear in Turning. *Advanced Engineering Research* (*Rostov-on-Don*). 2026;26(1):2103. https://doi.org/10.23947/2687-1653-2026-26-1-2103

Оригинальное теоретическое исследование

Вибрационное управление износом задней грани инструмента при точении

В.Е. Гвинджилия ✉
Донской государственный технический университет, г. Ростов-на-Дону, Российская Федерация
✉ vvgvindjiliya@donstu.ru

Аннотация

Введение. Интенсивностью износа режущего инструмента можно управлять, вводя дополнительные колебания в зону резания. Представляется достаточно изученным влияние параметров колебаний на износ инструмента. Однако выводы некоторых таких работ противоречивы. Отмечается, что вибрации с различной амплитудой могут как увеличивать износ, так и уменьшать его. В литературе нет аналитических моделей, разрешающих данное противоречие, отражающих нелинейную взаимосвязь подсистем инструмента и заготовки при резании. Кроме того, не принимается во внимание, что износу по разным граням инструмента требуются разные модели силового взаимодействия. Отмеченные пробелы восполняет представленная работа. Цель исследования — определить закономерности влияния высокочастотных колебаний (ВЧК) на износ задней грани инструмента.

Материалы и методы. Использовались данные математического моделирования динамической системы резания в Simulink с учетом сил по задней грани, эффективных параметров и ВЧК. Оборудование: станок 16К20, измерительный стенд вибрационного контроля с частотным диапазоном 0,4–15000 Гц, компьютер, аналого-цифровой преобразователь Е20–10, акустическая система, стенд для исследования сил резания — STD.201–1. Заготовки из стали 10ГН2МФА диаметром D = 84 мм обрабатывали инструментами с припаянными пластинами из Т15К6 без смазки.

Результаты исследования. Демонстрируется влияние ВЧК на силы контактного взаимодействия по задней грани инструмента и фазовая траектория деформационных смещений инструмента при разных амплитудах ВЧК: от $0{,}5 \cdot 10^{-2}$ до $2 \cdot 10^{-2}$ мм. Установлено, что мощность N необратимых преобразований энергии (НПЭ) зависит от направления вводимых вибраций. Показана зависимость интенсивности износа инструмента от дополнительных колебаний с амплитудами 5, 10 мкм в разных направлениях при скоростях резания 1 м/с, 1,4 м/с, 2 м/с. Полученные результаты сравниваются с траекториями износа без возмущения.

Обсуждение. Оптимальная амплитуда дополнительных вибраций в направлении подачи зависит от заднего угла инструмента и уменьшается с изменением стадии износа. Максимальное значение износа падает с 0,55 мм до 0,35 мм при введении колебаний с амплитудой 5 мкм и до 0,26 мм — при 10 мкм. При дополнительных вибрациях в тангенциальном направлении интенсивность износа слабо зависит от амплитуды вводимых колебаний, так как она во много раз меньше скорости колебательных смещений инструмента. Максимальное значение износа уменьшается с 0,65 мм до 0,6 мм при 5 мкм и до 0,48 мм — при 10 мкм. При интенсификации износа не существует оптимальной амплитуды дополнительных вибраций.

Заключение. Разработанные модели позволяют количественно оценивать влияние ВЧК на интенсивность износа инструмента по задней грани и обоснованно подбирать параметры колебаний, вводимых в зону резания. Так можно создавать:

– виртуальные модели процесса резания и подбирать режимы для минимизации скорости износа,

– системы мониторинга износа с комплексным подходом к прогнозированию.

Далее необходимо исследовать динамику процесса резания при амплитудах ВЧК более 10–15 мкм.

Ключевые слова: высокочастотные колебания, дополнительные колебания, динамическая система резания, износ инструмента, необратимые преобразования энергии

Благодарности. Автор выражает благодарность доктору технических наук, профессору В.Л. Заковоротному за плодотворные обсуждения и значимые рекомендации в процессе подготовки материала, а также сотрудникам лаборатории научно-исследовательского института «Вибротехнология» Донского государственного технического университета, оказавшим помощь при проведении научных экспериментов.

Финансирование. Работа выполнена в рамках соглашения на реализацию прикладного научного исследования «Разработка программно-аппаратных средств для мониторинга и анализа параметров резания и эксплуатационных характеристик станков с ЧПУ» (FZNE–2025–0008) № 075–03–2025–302/10 от 23.12.2025.

Для цитирования. Гвинджилия В.Е. Вибрационное управление износом задней грани инструмента при точении. *Advanced Engineering Research* (*Rostov-on-Don*). 2026;26(1):2103. https://doi.org/10.23947/2687-1653-2026-26-1-2103

Introduction. The impact of vibration on tool wear is the subject of numerous studies, as cutter wear determines the quality of parts and the efficiency of machining. The impact of vibrational oscillations on cutting force dynamics is comprehensively analyzed in the literature [1]. The diversity of tool and workpiece vibration sources and, correspondingly, the diversity of methods for monitoring, evaluating, and modeling them are noted [2].

At the initial stages of the development of cutting theory, vibrations were considered as a consequence of the loss of stability of the equilibrium of elastic deformations in a moving coordinate system, whose motion was determined by the trajectories of the machine actuators [3]. The loss of stability was associated with the effect of force regeneration [4], and a criterion for the stability of the equilibrium of elastic deformations [5] was proposed for its analysis. Regeneration problems were studied for turning [6], milling [7], drilling [8], and other operations.

The loss of stability was explained by:

– delay in force variations with changes in deformation [9];

– decreasing characteristic of force variation with increasing cutting velocity [10];

– regenerative effect of the tool mark on the workpiece [11];

– nonlinear dependence of the friction forces of the chip as it moves along the front face of the tool [12].

It is known [13] that when the trajectories of the tool formative movements lose stability, the most typical attracting sets for vibrations are those of the limit cycle [14] and the chaotic attractor [15]. It is established that changes in the attracting sets of tool vibrations are determined by the cutting conditions. For example, when changing the feed rate of the tool, all types of Andronov-Hopf bifurcations can be observed [16]. Vibrations were considered as a consequence of disturbances related to the quality of the machine tool. These were primarily spindle runout [17] and kinematic disturbances [18]. Depending on the frequency of external disturbances, various effects were observed [19]. At frequencies close to the natural frequencies of the interacting subsystems, parametric phenomena such as self-excitation, oscillation synchronization [20], and others, occur.

Finally, vibrations were studied as vibrations purposefully introduced into the cutting zone to achieve a beneficial effect: chip fragmentation [21], increased tool life [22], and improved surface quality [23]. It has been shown that introducing ultrasonic vibrations (USV) into the cutting zone can improve the quality of work and reduce the intensity of tool wear [24]. To improve the efficiency of USV, USV generation systems are proposed in which feedback for self-excitation is realized through vibrations generated under the cutting process [25]. In this case, nonlinear effects of the interaction between the tool and the workpiece are taken into account, specifically, the decreasing characteristic of cutting forces with increasing velocity [26] or the amplitude-frequency modulation of the system vibrations [27].

Researchers have paid particular attention to the impact of vibrations on the tool wear rate under cutting. It is widely believed that vibrations increase wear and thereby reduce tool life [23]. However, there is evidence that with an increase in the amplitude of the introduced vibrations, an optimum amplitude is recorded at which the wear rate reaches a minimum [28]. This effect is most pronounced when ultrasonic excitation is applied through the tool [28] and when turning difficult-to-machine materials such as AISI 52100 [29] or P9M4K8F [30].

To analyze the impact of vibrations on wear rate, methods and mathematical tools are needed that can allow for the rapid assessment of wear rate. It is advisable to use the power of irreversible energy transformations (PIET) in the contact zone of the tool and the workpiece as a diagnostic indicator [31]. When turning with tools with carbide inserts, the main type of wear is observed along the flank [32]. PIET is the primary source of heat generation, so it can be argued that the optimal cutting conditions correspond to the optimal temperature [33]. Heat production and PIET are correlated and adequately reflect wear rate [34]. Therefore, when developing wear monitoring systems, temperature and PIET in the cutting zone are considered as key diagnostic parameters. Diagnostic information models employ methods of autoregressive spectral analysis [35], models based on cutting force analysis using analytical functions [36], machine learning [37], and vibroacoustic emission signal analysis [38]. When the PIET changes, the mechanisms of physical and chemical interaction (wear) in the contact between the tool and the workpiece change — from adhesive-fatigue [1] and abrasive [31] to diffusion-oxidative [39].

PIET is often considered within the entire cutting zone. However, the power distribution between the tool flank, the chip formation zone, and the secondary plastic deformation zone is disproportionate. When analyzing flank wear rate, it is required to consider irreversible energy transformations in the contact area between the tool flank and the workpiece. It is not always taken into account that vibrations cause periodic changes in the power of irreversible transformations, and depending on the current power, various wear mechanisms are activated — from frictional fatigue to diffusion-oxidation. Consequently, estimates of the velocity and rate of tool wear change periodically. Furthermore, the literature does not describe the transformation of high-frequency vibrations (HFV) introduced into the cutting zone into the trajectories of the tool flank and the workpiece, nor into the trajectories of the forces generated in the contact zone.

The objective of this study is to establish the relationship between the HFV and tool flank wear rate based on a developed theoretical model of cutting dynamics, as well as its numerical and experimental analysis. To achieve this goal, the following work is being conducted to refine the models, simulate, and conduct theoretical studies and experiments.

1. Mathematical models of the dynamic cutting system (DCS) are refined. They are supplemented with constraints formed in the contact between the tool flank and the workpiece.

2. How the HFV introduced into the cutting zone are transformed into trajectories of the flank and workpiece, as well as into trajectories of forces generated in the contact zone, is studied. Numerical modeling of these processes is performed.

3. The changes in tool wear rate on the flank during longitudinal turning of 10GN2MFA steel are studied theoretically and experimentally. Their dependence on the ultrasonic waves introduced into the cutting zone is determined using the PIET analysis.

The developed mathematical tools and methods can be interpreted as the creation of a virtual numerical model of wear of cutting tools for the optimal selection of vibration parameters introduced into the cutting zone.

Materials and Methods

1. Problem statement. Mathematical modeling of DCS that takes into account forces on the tool flank. We consider the relationship between wear and PIET, as well as wear intensity patterns. To determine the PIET, we create a model of the DCS disturbed by the HFV. We develop algorithms and a program for calculating the PIET trajectories in the tool flank – workpiece contact (Fig. 1).

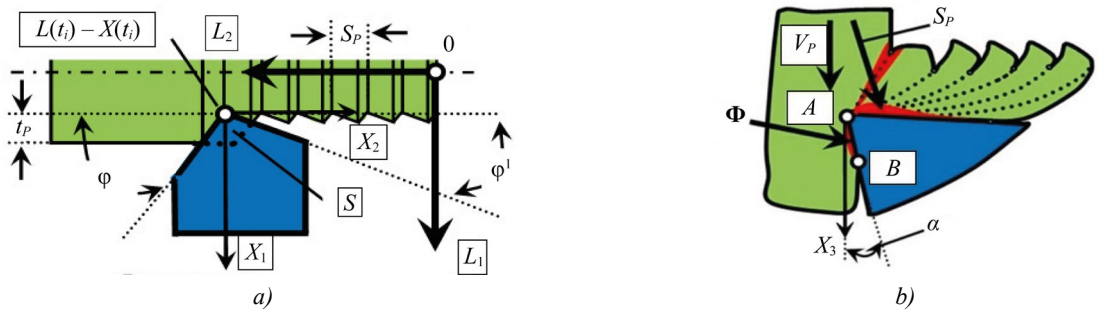

Fig. 1. Schematic diagram of the cutting process: *a* — representation of trajectories of actuators and deformation displacements; *b* — formation of cutting forces **F** in the region of primary and secondary plastic deformation, and additional forces **Φ** in the region *A* — *B*

Assume that the trajectories of the machine actuators are given in the form of displacements $\mathbf{L} = \{L_1, L_2, L_3\}^T \in \Re^{(3)}$ and velocities $\mathbf{dL/d} = \mathbf{V(t)}$, $\mathbf{V(t)} = \{V_1, V_2, V_3\}^T \in \Re^{(3)}$. Here, $L_1(t)$, $L_2(t)$ — trajectories of the transverse and longitudinal supports; $L_3(t) = \int_0^t \Omega(\xi) D(\xi) d\xi$ — displacements of the workpiece relative to the tool at the point of contact of the tool tip with the workpiece in the direction of its rotation; D — diameter of the machining surface, mm; d — diameter of the machined workpiece, mm (рис. 1).

The disturbances are characterized by displacements $\mathbf{\Delta X^{(X)}} = \{\Delta X_1^{(X)}, \Delta X_2^{(X)}, \Delta X_3^{(X)}\}^T \in \Re_{\mathbf{X}}^{(3)}$ and velocities $\mathbf{dX^{(X)}/dt} = \mathbf{\Delta V^{(X)}} = \{\Delta V_1^{(X)}, \Delta V_2^{(X)}, \Delta V_3^{(X)}\}^T \in \Re_{\mathbf{X}}^{(3)}$.

Let us consider the case when additional vibrations introduced into the cutting zone are represented by a vector of periodic disturbances: $\mathbf{\Delta X^{(X)}}(t) = \{\Delta X_{1,0}^{(X)} \sin(\Omega_\Delta t), \Delta X_2^{(X)} \sin(\Omega_\Delta t + \theta_2), \Delta X_3^{(X)} \sin(\Omega_\Delta t + \theta_3)\}^T \in \Re_{\mathbf{X}}^{(3)}$. Also — for velocities $\mathbf{\Delta V^{(X)}(t)} = \{\Delta X_{1,0}^{(X)} \Omega_\Delta \cos(\Omega_\Delta t), \Delta X_2^{(X)} \Omega_\Delta \cos(\Omega_\Delta t + \theta_2), \Delta X_3^{(X)} \Omega_\Delta \cos(\Omega_\Delta t + \theta_3)\}^T \in \Re_{\mathbf{X}}^{(3)}$.

Perturbations occur in the deformation space $\mathbf{X} = \{X_1, X_2, X_3\}^T \in \Re_{\mathbf{X}}^{(3)}$. Strain rates are $\mathbf{dX/dt} = \mathbf{V^{(X)}} = \{V_1^{(X)}, V_2^{(X)}, V_3^{(X)}\}^T \in \Re_{\mathbf{X}}^{(3)}$.

Vector $\mathbf{X}$ is considered in moving coordinates defined by $\boldsymbol{L}$ (Fig. 1). The unit of measurement for **L**, $\mathbf{\Delta X^{(X)}}$ and **X** — mm, for **V(t)**, $\mathbf{\Delta V^{(X)}}$ and $\mathbf{V^{(X)}}$ — mm/s.

The workpiece is rigid, so the trajectory of the shaping movements $\mathbf{L^{(\Phi)}} = \left\{L_1^{(\Phi)}, L_2^{(\Phi)}, L_3^{(\Phi)}\right\}^T \in \Re^{(3)}$ can be represented as:

$$\mathbf{L^{(\Phi)}} = \mathbf{L} + \mathbf{\Delta X^{(X)}} - \mathbf{X}. \quad (1)$$

We involve velocities $\mathbf{dL^{(\Phi)}/dt} = \mathbf{V^{(\Phi)}} = \mathbf{V} + \mathbf{\Delta V^{(X)}} - \mathbf{V^{(X)}}$ in the modeling. We use work [40] to indicate the relationship between forces and deformations:

$$\mathbf{m}\frac{\mathbf{d^2X}}{\mathbf{dt^2}} + \mathbf{h}\frac{\mathbf{dX}}{\mathbf{dt}} + \mathbf{cX} = \mathbf{F(L^{(\Phi)})} + \mathbf{\Phi(L^{(\Phi)})}. \quad (2)$$

Here, **m, h, c** — positive-definite symmetric matrices of inertial, velocity, and elastic coefficients, m = *diag*{*m*, *m*, *m*}. The dimensions of the matrix elements **m** — kg·s^2/mm, **h** — kg·s/mm, **c** — kgf/mm. $\mathbf{F(L^{(\Phi)})} = \left\{F_1, F_2, F_3\right\}^T \in \Re_{\mathbf{X}}^{(3)}$ — forces generated in the area of contact between the tool front face and the cutting zone. They depend on the dynamic properties in the areas of primary and secondary plastic deformation (highlighted in red in Fig. 1). $\mathbf{\Phi(L^{(\Phi)})} = \left\{\Phi_1, \Phi_2, \Phi_3\right\}^T \in \Re_{\mathbf{X}}^{(3)}$ — additional forces caused by the approach of the tool flank to the workpiece (region *A* — *B* in Fig. 1).

Forces $\mathbf{\Phi(L^{(\Phi)})}$, introduced additionally to the model considered in [10] reveal the interaction between the tool flank and the workpiece. They limit the development of periodic movements, generate forces acting on the flank, and, together with the trajectories $\mathbf{L^{(\Phi)}}$, determine the work and power of irreversible energy transformations in the contact area of the tool flank. Forces **F** and **Φ** are represented as functions of trajectories $\mathbf{L^{(\Phi)}}$, which vary depending on $\Delta X_i(t)$ and the elastic response of the tool $X_i(t)$.

Let us analyze processing with constant modes: $L_1 = L_1(0) = d/2 = const$.

Here, d — diameter of the processed workpiece under cutting (Fig. 1), $L_2(t) = V_2 t$, $V_2 = const$, $L_3(t) = V_3 t$, $V_3 = \pi D\Omega = const$.

Before we start modeling $\mathbf{F(L^{(\Phi)})}$, let us make three statements [41].

1. Forces **F** grow monotonically with increasing cutting area S (Fig. 1), which can be represented as: $S(t) = t_P(t)S_P(t)$. Here and hereafter $t_P(t)$, $S_P(t)$ — current values in mm of the cutting depth and the feed rate, respectively.

2. Vector **F** has the form: $\mathbf{F} = \{\chi_1, \chi_2, \chi_3\}^T$, where χ_i — angular coefficients, and $\{(\chi_1)^2 + (\chi_2)^2 + (\chi_3)^2\} = 1$.

3. There is a delay between the variations of **F** and S.

The delay is modeled by an aperiodic link with time constant $T^{(0)}$, which depends on the modes $t_P(t)$, $S_P(t)$, $V_P(t)$. Here, $V_P = \{(V_1)^2 + (V_2)^2 + (V_3)^2\}^{0.5}$ — cutting velocity. If there are no vibration disturbances and the deformation rates are small, then $V_P(t) \approx V_3$, since $V_2 \ll V_3$, and for longitudinal turning — $V_1 = 0$. When determining time constant $T^{(0)}$, called the chip formation time constant in [3], it is taken into account that the path traveled by the tool tip relative to the workpiece remains approximately constant [3]. In this case, the transition from one stationary state to another is considered.

The above means that $T^{(0)}$ depends mainly on the cutting velocity, and it can be approximated:

$$T^{(0)} = \frac{T_0^{(0)}}{1 + k^{(T)} V_3^{(\Phi)}}. \quad (3)$$

Here, $T^{(0)}$ — time constant in the region of low cutting speeds, s; $k^{(T)}$ — coefficient with the dimension s/mm.

According to [10], approximation (3) is valid in a limited range of variations of the process mode. For example, when processing 45 steel, the limitations are determined as $V_P \in (0.2; 2.5) \cdot 10^3$ mm/s. The greatest approximation error is observed in the range of low cutting velocities and depends mainly on the properties of the limit state of the material being processed, its plasticity and thermophysical characteristics. If the parameters are specified, then the following is valid:

$$T^{(0)}\left(V_3^{(\Phi)}\right)dF^{(0)}/dt + F^{(0)} = \rho\left\{t_P^{(0)} + \Delta X_1(t) - X_1(t)\right\}\left\{\int_{t-T}^{t}\left\{V_2 + \Delta V_2(\xi) - V_2^{(X)}(\xi)\right\}d\xi\right\}, \quad (4)$$

where T — workpiece turnover time, s; ρ — chip pressure on the front face of the tool, kg/mm^2.

To illustrate the analysis method, we limit ourselves to the case where the main and auxiliary angles in the tool plan are equal (Fig. 1): $\phi \Rightarrow \pi/2$, $\phi^1 \Rightarrow 0$.

Let us consider the disturbances: $\mathbf{\Delta V^{(X)}} = \{0, \Delta V_2^{(X)}, 0\}^T$ and $\mathbf{\Delta V^{(X)}} = \{0, 0, \Delta V_3^{(X)}\}^T$.

We exclude $\mathbf{\Delta V^{(X)}} = \{\Delta V_1^{(X)}, 0, 0\}^T$ from the analysis since $S_P \ll t_P$. Moreover, the internal gain in the self-excitation channel varies significantly depending on the deformation direction. For the direction X_1, the gain will be an order of magnitude smaller than for X_2. Furthermore, with the tool geometry under consideration, it is precisely the vibrations in $X_2 - X_3$ plane that bring the tool flank and the workpiece closer together, which determines the intensity of wear and generates additional forces $\mathbf{\Phi(L^{(\Phi)})}$.

Thus, if $\Omega = const$, $dX_3/dt \to 0$ and $d\Delta X_3(t)/dt \to 0$, then $T = (\Omega)^{-1}$. Otherwise, T is required to calculate from the ratio:

$$T\left(L_3^{(\phi)}\right) = \int_{L_3^{(\phi)} - \pi D}^{L_3^{(\phi)}} \frac{d\xi}{V_P(\xi)} \tag{5}$$

Here, V_P — law of cutting velocity variation, taking into account elastic deformations and disturbances. To study the PIET, it is necessary to know the force model $\mathbf{\Phi(L^{(\Phi)})}$. After cutting-in (Fig. 2 *a*), a trace trajectory is formed on the workpiece at angle $\varphi = arctg(V_3/V_2)$ (Fig. 2 *b*).

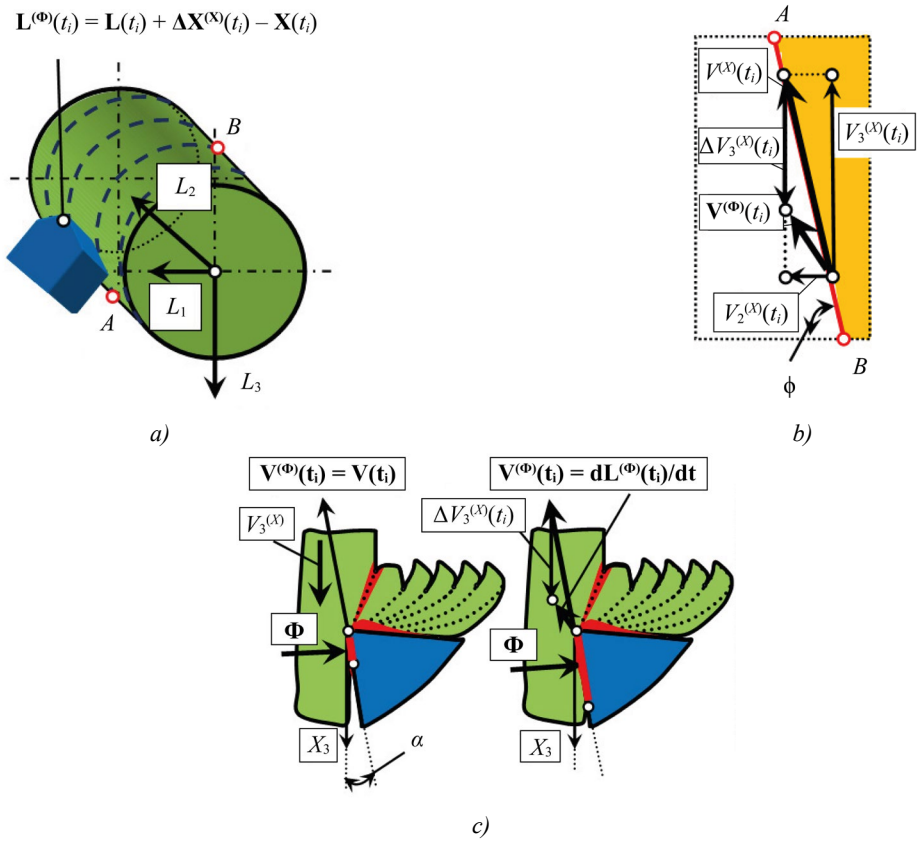

Fig. 2. Forces $\mathbf{\Phi(L^{(\Phi)})}$ generation diagram: *a* — formation of a tool mark on the workpiece surface; *b* — change in direction of movement when velocity and direction of rotation of the workpiece coincide; *c* — convergence of the surfaces of tool flank and workpiece when the direction of movement of the velocity $\mathbf{V^{(\Phi)}}(t_i)$ changes

Direction ϕ is indicated by the line *A* — *B* (Figs. 1, 2). When changing $V_3^{(X)}$, as shown in Figure 2 *b*, due to $\Delta V_3^{(X)}$, the direction of the tool movement towards or away from the workpiece changes. As the surfaces approach each other, the forces on the flank increase. When vector $V^{(X)}$ shifts to the area highlighted in yellow (Fig. 2 *b*), the tool moves away from the workpiece, and area *S* decreases. If the equilibrium position of elastic deformations is stable and unperturbed, then the trajectory of movement in the direction *A* — *B* (Fig. 2) is an attractor. It is displaced in space **L** by a constant amount of elastic deformation. Due to disturbances or loss of stability, periodic convergence or repulsion of the flanks from the workpiece occurs. To estimate the deviation of the trajectory from the projected attractor, it is convenient to consider dimensionless aggregated coordinates:

$$\upsilon(t) = \left(V_2 + \Delta V_2^{(X)}(t) - dX_2/dt\right) / \left(V_3 + \Delta V_3^{(X)}(t) - dX_3/dt\right); \upsilon^* = V_2/V_3. \tag{6}$$

Here, $\upsilon(t)$ — dimensionless aggregated coordinate defining the current position of the direction of the tool tip movement; υ^* — aggregated coordinate defining the desired direction of tool movement, specified by velocities V_2 and V_3.

The approach of the flank to the workpiece surface depends on the kinematic value of the clearance angle α. The experiments described in [39] show that forces $\mathbf{\Phi(L^{(\Phi)})}$ increase disproportionately with decreasing α according to an exponential law. Therefore:

$$\begin{aligned}\Phi_2 &= k_\Phi F_0 + \rho_0\left[t_P^{(0)} - X_1(t)\right]exp\left[\varsigma\left(\upsilon-\upsilon^*\right)\right],\\ \Phi_3 &= k_\Phi k_T F_0 + k_T\rho_0\left\{\left(t_P^{(0)} - X_1(t)\right)exp\left[\varsigma\left(\upsilon-\upsilon^*\right)\right]\right\},\end{aligned} \tag{7}$$

where ρ_0 — coefficient of conversion of contact length into force, kg/mm; ς — dimensionless parameter dependent on the tool clearance angle α in statics; k_T — dimensionless coefficient of friction; k_Φ — dimensionless coefficient that determines the elastic recovery of the material.

From (7), it follows that there is a potential relationship between deformations and disturbances in the direction of trajectories *A* — *B* (Fig. 2), and they have virtually no effect on the forces generated at the contact between the tool flank and the workpiece. In this case, variations in cutting velocity in the range of actual values will be small. Let us denote the current variations in velocities in the directions X_2 and X_3: $\delta V_2 = \Delta V_2^{(X)}(t) - V_2^{(X)}(t)$, $\delta V_3 = \Delta V_3^{(X)}(t) - V_3^{(X)}(t)$. Then from (6), we obtain:

$$V_3\delta V_2^{(X)}(t) = V_2\delta V_3^{(X)}(t). \tag{8}$$

Let us consider harmonic disturbances in two orthogonal directions, maintaining the ratio between the amplitudes of the additional vibrations. In this case, the in-phase condition of vibration (8) is $V_3/V_2 = \delta V_3/\delta V_2$. It is almost never satisfied in the dynamic cutting system. There are two reasons for this. Firstly, $V_2 \ll V_3$, therefore, the direction of the total vibrations (i.e., vibrations introduced into the cutting zone with regard to deformation displacements) must be oriented along the direction of the cutting velocity. Secondly, it is important to consider the response from the cutting process. Then the total stiffness matrices of the tool subsystem become asymmetrical, even if we neglect the forces generated by the matrices **m** and **h**. Skew-symmetric components of the elasticity matrices generate circulatory forces that cause precessional movements of the tool relative to the workpiece. It has been experimentally established [39] that this form of vibrations always occurs. It provides phase displacements between vibrations in two orthogonal directions. Due to the asynchronous nature of the vibrations in the two orthogonal directions, periodically repeating sections are formed in which the tool flank and the workpiece are observed approaching each other. This occurs even with small variations in velocity relative to the established cutting velocity.

To determine the PIET, it is required to calculate the forces and vibrational velocities. Obviously, the PIET depends not only on the parameters introduced into the cutting zone of vibrations, but also on the dynamic properties of the entire USV. If we consider the interactions in terms of nonlinear acoustics, then the efficiency of ultrasonic vibration under cutting is determined by the acoustic impedance of the medium into which the ultrasonic vibrations are introduced [28]. In our case, this corresponds to the dynamic properties of the cutting system.

2. Mathematical modeling of effective parameters and forces. If we follow the paradigm of mesomechanics [42], then variation of the properties of the dynamic coupling formed by cutting, due to the introduction of HFV into the cutting zone, should be characterized by molecular-mechanical effects that change the properties of the system at the macro level. By frequency range at the macro level, we mean the range within the passbands of the interacting subsystems $\mathbf{\Omega^{(0)}} \in (0, \Omega_c)$, where Ω_c — cutoff frequency of the DCS.

Note that the macrosystem does not perceive HFV in the frequency range $\mathbf{\Omega^{(0)}}$, but they do change its properties. To explain this transformation, let us recall the cutting process and the dynamic coupling in the system of mechanical interactions (2). HFV contribute to the transformation of the parameters of this coupling, and subsequently — to the change in the macrosystem. This is known from the description of the averaging method in the theory of nonlinear vibrations [43].

The basic parameters affecting the properties of the system are ρ and $T^{(0)}$ [6]. A typical example of effective parameters is the dimensionless effective friction coefficient k_T, studied in [42]. The effective value of k_T can change and even reverse sign under vibrations. This depends on the trajectory of the HFV introduced into the contact area.

Let us describe the conditions for determining the effective value of k_T. For this purpose, the relationship between two factors is determined:

– the tangential forces of contact interaction;

– variations in their normal components.

For analysis, a frequency region within the passband of the interacting subsystems of the tool and workpiece is selected. The analysis time is the period of high-frequency vibrations.

Let us consider parameter ρ. Additional vibrations create a stress state that changes cyclically in the primary plastic deformation zone. The limit state of the material practically does not change, it remains close to its ultimate strength [44]. Integral and cyclic loads are redistributed, causing changes in the effective values of $\hat{\rho}$. Moreover, the dynamic bond formed by the cutting process lacks central symmetry with respect to deformations in the neighborhood of the equilibrium position. As a result, a complex stress state arises in the cutting zone, described by additional constant and cyclic force components. Assuming the ultimate limit state of the material is maintained in the cutting zone, we obtain the effective value of $\hat{\rho}$:

$$\hat{\rho} = \rho\left(1-\varepsilon_\rho\right), \tag{9}$$

where $\varepsilon_\rho = \hat{\rho}^{(C)} / \rho$ — dimensionless parameter; $\hat{\rho}^{(C)} = \Omega_\Delta \int_{t-(\Omega_\Delta)^{-1}}^{t} \rho(\xi) d(\xi)$; $\Omega_\Delta \in \mathbf{\Omega}^{(\Delta)}$.

It is obvious that $\varepsilon_\rho \langle 1$.

Let us estimate the effective value of $\hat{T}^{(0)}$ taking into account (3). The specified vibrations $\delta V_3(t) = \Delta V_3^{(X)}(t) - V_3^{(X)}(t)$ are independent of the vibration power. The period of the function $\delta V_3(t)$ is generally determined by the period of the vibrations $T_\Delta = (\Omega_\Delta)^{-1}$. That is, due to the introduced vibrations, attracting sets of the limit cycle type are formed in the dynamic cutting system. Moreover, Ω_Δ is at least an order of magnitude higher than the upper natural frequency of the vibrational circuits formed by the tool subsystem. We expand the nonlinear function $T^{(0)}(V_3, \delta V_3)$ in a Taylor series in the neighborhood of δV_3:

$$T^{(0)}\left(V_3,\delta V_3\right) = T_0^{(0)}\left(V_3,0\right) + \frac{\partial T_0^{(0)}}{\partial \delta V_3}\delta V_3 + \frac{1}{2!}\frac{\partial^2 T_0^{(0)}}{\left(\partial \delta V_3\right)^2}\left(\delta V_3\right)^2 + \ldots \tag{10}$$

With $\delta V_3 \ll V_3$, series (10) converges quickly, therefore we limit ourselves to a linear approximation of the dependence of the time constant T_0 on additional vibrations, that is, from (10) we obtain:

$$T_0\left(V_3,\delta V_3\right) = \frac{T_0^{(0)}}{1+k^{(T)}V_3} - \frac{k^{(T)}T_0^{(0)}\delta V_3}{\left[1+k^{(T)}V_3+k^{(T)}\delta V_3\right]^2}. \tag{11}$$

In (10), the first term is a constant value at $V_3 = const$. Function $\Delta\left(V_3,\delta V_3\right) = \frac{k^{(T)}\delta V_3}{\left[1+k^{(T)}V_3+k^{(T)}\delta V_3\right]^2}$ is periodic, with a period of T_Δ, and $(T_\Delta)^{-1} = \Omega_\Delta \in \mathbf{\Omega_\Delta}$. Therefore, to determine the effective value of $\hat{T}_0(V_3,\delta V_3)$, the following is valid:

$$\hat{T}_0\left(V_3,\delta V_3\right) = T_0^{(0)}\left\{\frac{1}{1+k^{(T)}V_3} - \Delta\left(V_3,\delta V_3\right)\right\}, \tag{12}$$

where $\Delta = \frac{1}{T_\Delta}\int_{t-T_\Delta}^{t}\left\{\frac{k^{(T)}T_0^{(0)}\delta V_3}{\left[1+k^{(T)}V_3+k^{(T)}\delta V_3\right]^2}\right\}d\xi$.

Thus, we see what happens when vibrations that are not directly transmitted by the tool and workpiece subsystems are introduced into the cutting zone. In this case, the parameters of the dynamic coupling formed by the cutting process change.

The system equilibrium is asymptotically stable and unperturbed. The time constant T_0 at $V_3 = const$ is also constant and is determined from the expression $T_0 = \frac{T_0^{(0)}}{1+k^{(T)}V_3}$. Otherwise, the HFV is changed. This transformation is determined by the ratio of the vibrational velocity amplitude to the cutting velocity, which is taken into account by Δ in (12). Thus, HFV change the system properties in the low-frequency region. For example, increasing the time constant $\hat{T}_0$ has two effects on equilibrium stability:

– it causes additional phase displacements between deformations and forces, which contributes to instability;

– it promotes damping of vibrations, which increases stability.

In all cases, as the amplitude increases, a decrease in the effective values of the parameters $\hat{\rho}$ and $\hat{T}_0$ is observed. Their variation affects the stability of the controlled trajectories and the dynamic properties of the system in the frequency domain $\mathbf{\Omega^{(0)}}$. This, in turn, affects the attractive sets of deformation displacements of the tool relative to the workpiece.

3. Mathematical modeling of the impact of the HFV on the cutting forces at the flank. Vibrations change the interactions between the tool flank and the workpiece (7). They also cause reactions outside the bandwidth of the system represented by (2). Therefore, forces **Φ** must also be taken as averages over the vibration period. Let us analyze the effect of vibrations on Φ_2. Forces Φ_3 differ by a factor of k_T. Consider two cases for an asymptotically stable system.

The first case: the vibrations are determined by the velocities in the feed direction $\Delta V_2^{(X)} sin(\Omega_0 t)$ and represent the difference between the vibrational velocities introduced into the cutting zone and the deformation velocities. Then from (7), we obtain:

$$\Phi_2 = \rho_0\left[t_P^{(0)} - X_1\right]\left\{exp\left[\varsigma(\upsilon-\upsilon^*)\right]\right\} = \rho_0\left[\left(t_P^{(0)} - X_1(t)\right)\right]\left\{exp\left[\varsigma\frac{\Delta V_2^{(X)}\, sin(\Omega_0 t)}{V_3^{(X)}}\right]\right\}.$$

As before, we expand $exp\left[\varsigma\frac{\Delta V_2^{(X)}\, sin(\Omega_0 t)}{V_3^{(X)}}\right]$ in a Taylor series:

$$\Phi_2\left(A_{X_2}\, sin(\Omega_0 t)\right) = \Phi_2^*\left\{1 + A_{X_2}\, sin(\Omega_0 t) + \frac{1}{2!}\left[A_{X_2}\, sin(\Omega_0 t)\right]^2 + \frac{1}{3!}\left[A_{X_2}\, sin(\Omega_0 t)\right]^3 + ... + \frac{1}{n!}\left[A_{X_2}\, sin(\Omega_0 t)\right]^n + ...\right\},$$

where $\Phi_2^* = \rho_0\left[t_P^{(0)} - X_1\right]$; $A_{X_2} = \varsigma\frac{\Delta V_2^{(X)}}{V_3^{(X)}}$.

The region of convergence of the series is $-\infty\langle A_{X_2}\sin(\Omega_0 t)\langle+\infty$. We average $\Phi_2\left(A_{X_2}\, sin(\Omega_0 t)\right)$ over the period $(\Omega_0)^{-1}$ and limit ourselves to the first four terms of the series:

$$\hat{\Phi}_2\left(A_{X_2}\right) = \rho_0\left[t_P^{(0)} - X_1\right]\left\{1 + \frac{1}{4}\left[A_{X_2}\right]^2 + \frac{3}{48}\left[A_{X_2}\right]^4\right\}. \quad (13)$$

This series always converges. The system is stable. Therefore, for $A_{X_2} = 0$, $\Phi_2(\upsilon)_{\upsilon=\upsilon^*} = \rho_0\left[t_P^{(0)} - X_1\right]\left\{exp\left[\varsigma(\upsilon-\upsilon^*)\right]\right\} = \rho_0\left[t_P^{(0)} - X_1\right]$. As $\Delta V_2^{(X)}$ increases, a growth of the effective value of $\hat{\Phi}_2(A_{X_2})$ is observed, which depends on $V_3^{(X)}$. This component is perceived by the subsystems and is within their bandwidth. This allows us to introduce the concept of latent force:

$$\Phi_2^{(C)}\left(\Delta V_2^{(X)}\, sin(\Omega_0 t)\right) = \rho_0\left[t_P^{(0)} - X_1(t)\right]\left\{exp\left[A_{X_2}\, sin(\Omega_0 t)\right] - 1 - \frac{1}{4}\left[A_{X_2}\right]^2 - \frac{3}{48}\left[A_{X_2}\right]^4\right\}. \quad (14)$$

It is obvious that with $\Delta V_2^{(X)} = 0$, force $\Phi_2^{(C)} = 0$.

The second case: the vibrational velocities are equal to $\Delta V_3^{(X)} sin(\Omega_0 t)$, and $\Phi_2 = \rho_0\left[t_P^{(0)} - X_1(t)\right]\left\{exp\left[\varsigma(\upsilon-\upsilon^*)\right]\right\}$. Expression $(\upsilon-\upsilon^*) = -\frac{V_2^{(X)}}{V_3^{(X)}}\frac{\Delta V_3^{(X)}\, sin(\Omega_0 t)}{\left(V_3^{(X)} + \Delta V_3^{(X)}\, sin(\Omega_0 t)\right)}$ is expanded in a Taylor series:

$$(\upsilon-\upsilon^*) = -\frac{V_2^{(X)}}{V_3^{(X)}}\varepsilon_{V_3}\, sin(\Omega_0 t)\left\{1 - \varepsilon_{V_3}\, sin(\Omega_0 t) + \left[\varepsilon_{V_3}\, sin(\Omega_0 t)\right]^2 - ... + (-1)^n\left[\varepsilon_{V_3}\, sin(\Omega_0 t)\right]^n + ...\right\}, \quad (15)$$

where $\varepsilon_{V_3} = \Delta V_3^{(X)} / V_3^{(X)}$.

Series (15) converges quickly since $\varepsilon_{V_3}\langle 1$. We average the expression over the period $(\Omega_0)^{-1}$ and limit ourselves to four terms:

$$\hat{\Phi}_2\left(\varepsilon_{V_3}\right) = \rho_0\left[t_P^{(0)} - X_1(t)\right]\left\{exp\left[\varsigma\frac{V_2^{(X)}}{V_3^{(X)}}\left(\frac{1}{2}\left(\varepsilon_{V_3}\right)^2 + \frac{3}{8}\left(\varepsilon_{V_3}\right)^4\right)\right]\right\}. \quad (16)$$

At $\Delta V_2^{(X)} = \Delta V_3^{(X)} = 0$, expressions $\hat{\Phi}_2(A_{X_2})$ and $\hat{\Phi}_2(\varepsilon_{V_3})$ are transformed into (7) without taking into account forces $k_\Phi F_0$. Effective values of $\hat{\Phi}_2(A_{X_2})$ and $\hat{\Phi}_2(\varepsilon_{V_3})$ differ due to the direction of vibrations — X_2 or X_3. In the first case, vibrations change the proximity of the flank and the workpiece, while in the second, they change the projections of the vector onto the direction X_2.

Here, we can also consider the latent force, which is zero in a stable system ($\Delta V_3^{(X)} = 0$):

$$\Phi_2^{(C)}\left(\Delta V_3^{(X)}\, sin(\Omega_0 t)\right) = \rho_0\left[t_P^{(0)} - X_1(t)\right]\left\{\begin{array}{l} exp\left[-\varsigma\frac{V_2^{(X)}}{V_3^{(X)}}\frac{\Delta V_3^{(X)}\, sin(\Omega_0 t)}{\left(V_3^{(X)} + \Delta V_3^{(X)}\, sin(\Omega_0 t)\right)}\right] - \\ -exp\left[-\varsigma\frac{V_2^{(X)}}{V_3^{(X)}}\left(\frac{1}{2}\left(\varepsilon_{V_3}\right)^2 + \frac{3}{8}\left(\varepsilon_{V_3}\right)^4\right)\right] \end{array}\right\}. \quad (17)$$

The presented analysis allows us to formulate two conclusions that are important for further work.

1. Tool flank wear depends on the direction of the HFV. For example, forces Φ_2 increase significantly more when vibrations are excited in the feed direction, and the rate of their increase depends on ς. Parameter ς increases with decreasing tool clearance angle α and as wear progresses.

2. Changes in the PIET and effective forces upon excitation of additional vibrations cause a displacement in the equilibrium of deformations affecting the diameter of the workpiece. Thus, the parameters of the HFV characterize the control parameters that change the properties of the system, including tool wear rate and surface quality.

4. Experiment Design and Simulation Parameters. The experiments were performed on a 16K20 machine tool with an adjustable spindle rotation and carriage feed drive. A603C01 vibration accelerometers with a sensitivity of 10.2 mV/(m/s²) and a frequency range of 0.4–15000 Hz were used as measurement interfaces. They were mounted on the tool in the longitudinal and tangential directions. The measuring stand collected data and transmitted it to the computer via an E20–10 analog-to-digital converter (ADC) with a sampling frequency of 100 kHz. The data obtained was processed using low-pass filtering algorithms to suppress noise in the measuring circuit. To determine the vibrational velocities and tool tip displacements, the vibration acceleration signal was integrated by software methods with trend removal. To measure forces, the STD.201–1 measuring system was installed in place of the support, which included:

– unit for measuring dynamic tool loads along axes $\{X_1, X_2, X_3\}$;

– interface unit for collecting and transmitting data.

The latter consisted of electronic units manufactured by National Instruments (USA): NI-9234, Ni-9237, and NI-9219. The sampling frequency was up to 50 kHz. The National Instruments system also measured the integral temperature value in the cutting zone. This indicator was associated with the power of irreversible energy transformations throughout the cutting zone.

To introduce USV into the cutting zone, an acoustic system based on a 500-watt magnetostrictive transducer was used, powered by a 1.5-kW ultrasonic generator. The device for automatically adjusting the generator frequency to the resonance of the acoustic system shifted when the boundary conditions of the tool – workpiece interface changed under the cutting process. Vibrations were measured with an accelerometer. Their intensity was estimated from the amplitude of harmonic displacements at a frequency of Ω_0. Workpieces made of 10GN2MFA steel were machined using tools with brazed T15K6 plates without the cutting fluid.

The computer simulation considered disturbances $\Delta V_2^{(X)} sin(\Omega_0 t)$ and $\Delta V_3^{(X)} sin(\Omega_0 t)$, $\Omega_0 = (5 – 20)$ kHz.

The main angles of the T15K6 tool were $\phi = 90°$, $\phi^1 = 30°$ and $\alpha = 6°$ (Fig. 1). These values were selected to simplify the modeling of the dynamic cutting system, since at $\phi = 90$, forces generated in the area of tool – workpiece contact produced practically zero projections in the direction X_1.

Process modes without considering deformations and disturbances were:

– feed rate $S_P^{(0)} = 0.1$ mm/rev;

– depth $t_P^{(0)} = 2$ mm;

– cutting velocity $V_P^{(0)} = (0.5 – 3.8)\cdot 10^3$ mm/s.

When varying $V_P^{(0)}$, the ratio of workpiece rotation velocity to longitudinal feed rate was maintained so that $t_P^{(0)} = const$. The tool subsystem parameters are given in Table 1. The total mass was $m = 0.015$ kg·s²/mm.

Table 1

Matrices of Velocity Coefficients and Tool Subsystem Elasticity [40]

Matrix element	Value, kg/mm	Matrix element	Value, kg·s/mm
$c_{1,1}$	200	$h_{1,1}$	1.3
$c_{2,2}$	900	$h_{2,2}$	1.1
$c_{3,3}$	350	$h_{3,3}$	0.8
$c_{1,2} = c_{2,1}$	200	$h_{1,2} = h_{2,1}$	0.6
$c_{1,3} = c_{3,1}$	150	$h_{1,3} = h_{3,1}$	0.5
$c_{2,3} = c_{3,2}$	80	$h_{2,3} = h_{3,2}$	0.4

The dynamic coupling parameters (Table 2) were determined experimentally by methods and programs described in detail for the parameters of high-speed [45] and positional [46] communication.

Table 2

Dynamic Coupling Parameters

ρ, kg/mm^2	ρ_0, kg/mm	Ω, Hz	$T_0^{(0)}$, s	ς	k_T	$k^{(T)}$, s/m	$k^{(S)}$	χ_1	χ_2	χ_3
100–1000	20	5–50	0.0001	1–7	0.2	5	0.1	0.4	0.51	0.76

Work A and power N are scalar quantities. They depend on the direction of movement and are measured in kg·mm and kg·mm/s, respectively. Let us consider A and N in the direction A — B (Fig. 2). When turning, $V_2/V_3 \Rightarrow 0$. This means:

$$N(t) = \Phi_2(t)V_2,\ A(t) = V_2\int_0^t \Phi_2(\xi)d\xi(a),$$

$$N(t) = \Phi_3(t)V_3^{(\Phi)}(t),\ A(t) = \int_0^t \Phi_3(\xi)V_3^{(\Phi)}(\xi)d\xi(б). \quad (18)$$

Here, a — power N and work A in the feed direction; b — power N and work A in the direction of velocity V_3.

The cutting process dynamics modeling [47] demonstrated the validity of the sensitivity analysis of force variations to deformations in the feed direction. Furthermore, a regenerative self-excitation effect was formed in the direction X_2, affecting the dynamics of the approach of the tool flank to the workpiece.

The numerical simulation of turning a shaft with a diameter of D = 84 mm was performed in the Simulink software package. This example can be used to study the vibration control of the PIET.

Research Results. Let us examine the results of vibration control of the power of irreversible energy transformations in the feed direction (18a) under the impact of high-frequency vibrations. First, we analyze the dependence of $\Phi_2(t)$ on $\Delta X_2^{(X)} sin(\Omega_0 t)$ without considering $k_\Phi F_0$ (Fig. 3 a).

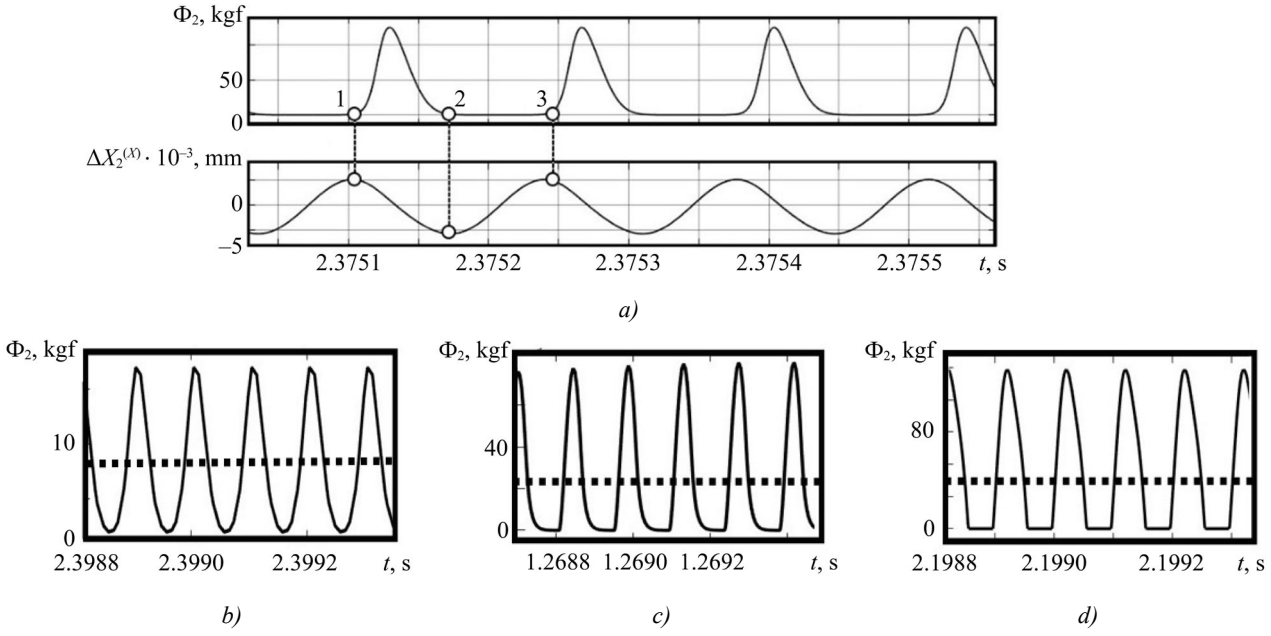

Fig. 3. Example of change in trajectories of force $\Phi_2(t)$: a — joint trajectories of forces and vibrations with a change in HFV $\Delta X_2^{(X)}$ without considering $k_\Phi F_0$; b — change in trajectories of forces with an amplitude of $\Delta X_2^{(X)} = 0{,}7 \cdot 10^{-3}$ mm; c — $\Delta X_2^{(X)} = 1 \cdot 10^{-2}$ mm; d — $\Delta X_2^{(X)} = 2 \cdot 10^{-2}$ mm

Note the nonlinear distortions of $\Phi_2(t)$. They increase at $\Delta V_2^{(X)}(t)$, directed toward the flank and workpiece (section 1–2) and are practically zero when its sign changes (section 2–3). At small amplitudes (Fig. 3 a), the force variations are almost harmonic. The nonlinear distortions are due to nonlinear relationship (7), which does not have central symmetry at any point.

As we can see, the disproportionate increase in the force impulse varies depending on the clearance angle α. At small angles (large ς), a rapid increase is observed even at low amplitudes of the HFV.

Next, we analyze the relationship between the forced HFV and the tangential components of the contact interaction forces (Fig. 4).

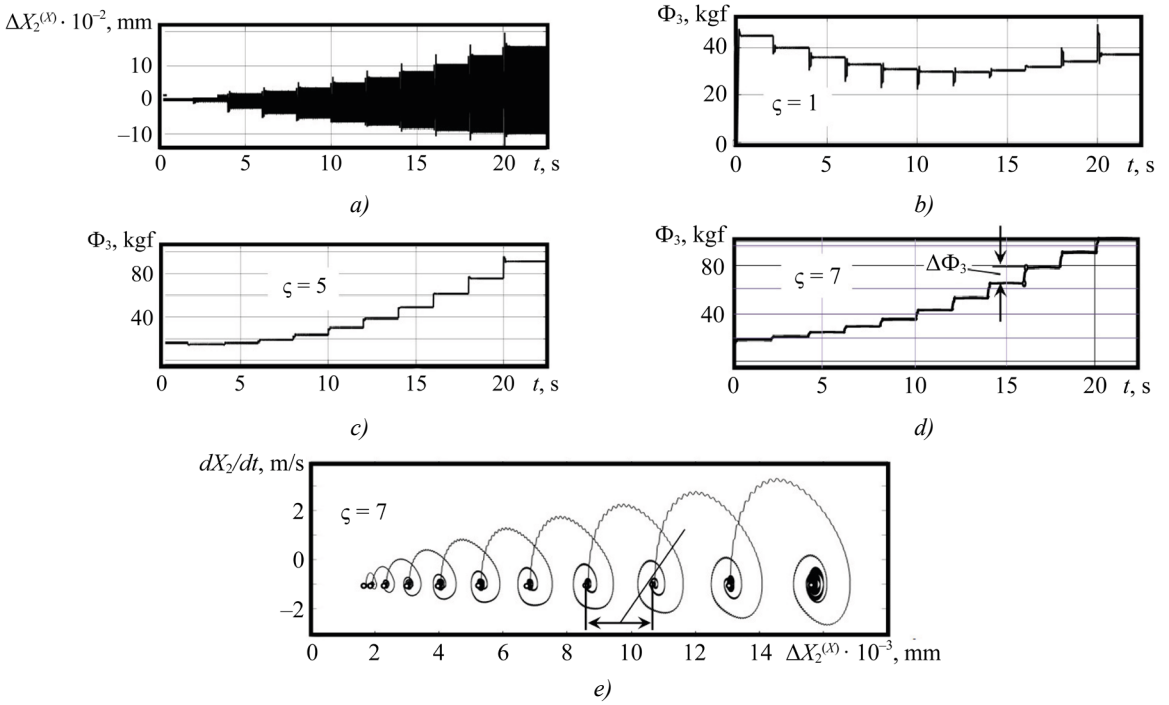

Fig. 4. Example of impact of forced HFV on tangential components of contact interaction forces: *a* — trajectories of forced vibrations; *b* — trajectory of Φ_3 at $\varsigma = 1$; *c* — trajectory of Φ_3 at $\varsigma = 5$; *d* — trajectory of Φ_3 at $\varsigma = 7$; *e* — example of phase trajectory of tool deformations considering vibration disturbances

The change in the amplitude of the HFV $\Delta X_2^{(X)}$ in Figure 4 *a* was specified by two piecewise constant functions with the duration of each step of Δt_{step}= 2 s:

– for the interval $t \in [0;8]$, the change in the amplitude of the first function was specified from 0 to $1.5 \cdot 10^{-2}$ mm for $t \in [0;8]$ with a step of $0.5 \cdot 10^{-2}$ mm;

– for the interval $t \in (8;22]$, the change in the amplitude of the second function was specified from $2 \cdot 10^{-2}$ mm to $14 \cdot 10^{-2}$ mm with a step of $2 \cdot 10^{-2}$ mm.

The arrows in Figure 4 *d*, *e* indicate the increment of forces $\Delta\Phi_3$ with increasing HFV amplitude and the corresponding displacement of the equilibrium point of the system in the phase plane.

Figure 4 *e* shows an example of the phase trajectory $X_2 - dX_2/dt$, corresponding to the change in force in Figure 4 *d*. Transient processes are caused by a jump in the amplitude. The equilibrium point ΔX_2^* shifts because the vibrations affect $\hat{\rho}$ and $\widehat{\mathbf{\Phi}}$.

According to [10], the main wear mechanisms change with increasing V_3 (increasing PIET). At low V_3, abrasive and adhesive-fatigue 10are observed, and with increasing V_3 — diffusion and oxidative wear. The transition from adhesive-fatigue to diffusion-oxidative wear corresponds to the minimum intensity. When vibrations are excited, the formation of PIET in the contact becomes more complex, however, wear rate can also be estimated from PIET.

Let us clarify the concepts of wear rate $v^{(L)} = dw/dL$ and velocity $v^{(t)} = dw/dt$. The magnitude of wear on the flank is usually considered as the equivalent width of the wear band w in mm, which is determined by the height of the equivalent rectangle of the wear scar on the flank. Equivalence is equality of areas, therefore:

$$v^{(L)} = v^{(t)} \left(V_p\right)^{-1}, \tag{19}$$

where $v^{(L)}$ is a dimensionless quantity.

In the velocity range of 0.7–3 m/s, dependence $v^{(L)}(N)$ is well approximated by the expression:

$$v^{(L)}(t) = \alpha^w \left\{1.8 + \beta^{(w)} \left[N(t) - 600\right]^2\right\}. \tag{20}$$

Here, $\alpha^{(w)}$ — dimensionless quantity; $\beta^{(w)}$ — parameter of dimension W^2. When processing heat-resistant steels, $\alpha^{(w)} = (0{,}9 - 1{,}1) \cdot 10^{-7}$. Due to vibrations, N becomes a function of time $N(t)$ with interrelated periodic and constant components. All physical interactions are inertial, that is, their manifestation also depends on frequency. Therefore, to estimate $N(t)$, it makes sense to introduce values $\hat{N}^{(X_2)}(\Delta X_2 \Omega_0)$, $\hat{N}^{(X_3)}(\Delta X_3 \Omega_0)$ depending on the direction of vibrations. For this, it is convenient to use the moving average operator for (20):

$$\hat{N}^{(X_i)}\left(\Delta X_2 \Omega_0\right) = \frac{\alpha^{(w)}}{T^{(X_i)}} \int\limits_{t-T^{X_2}}^{t} \left\{1.8 + \beta^{(w)} \left[N(\xi) - 600\right]^2\right\} d\xi, i = 2,3. \tag{21}$$

It is convenient to consider the averaging time as a multiple of the period $(\Omega_0)^{-1}$. Let us analyze the change in the PIET depending on the vibration amplitude at Ω_0 = 10 kHz. Let us consider its change depending on the HFV amplitude in the directions X_2 (Fig. 5 *a*) and X_3 (Fig. 5 *b*).

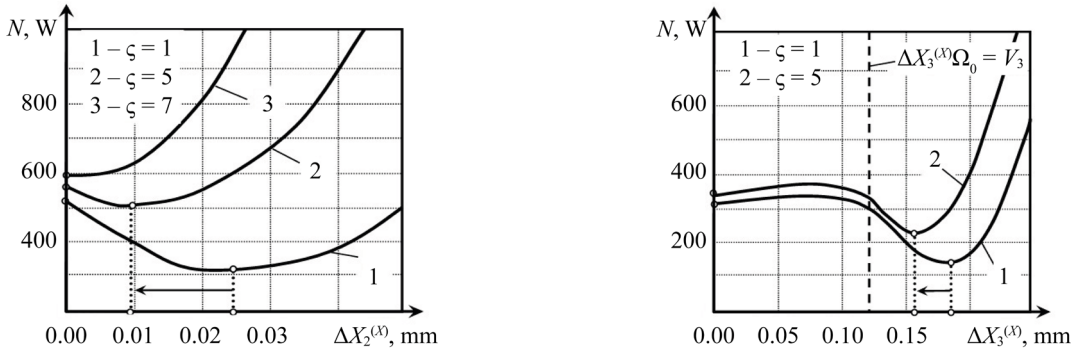

Fig. 5. Effect of vibrations on N: *a* — change in N depending on amplitude in the direction X_2; *b* — change in N depending on amplitude in the direction X_3

We see the HFV amplitudes at which the PIET reaches its minimum value, with the minimum depending on the degree of plate wear ς.

Figure 6 *a* shows the changes in $v^{(L)}$ depending on the PIET without additional vibrations.

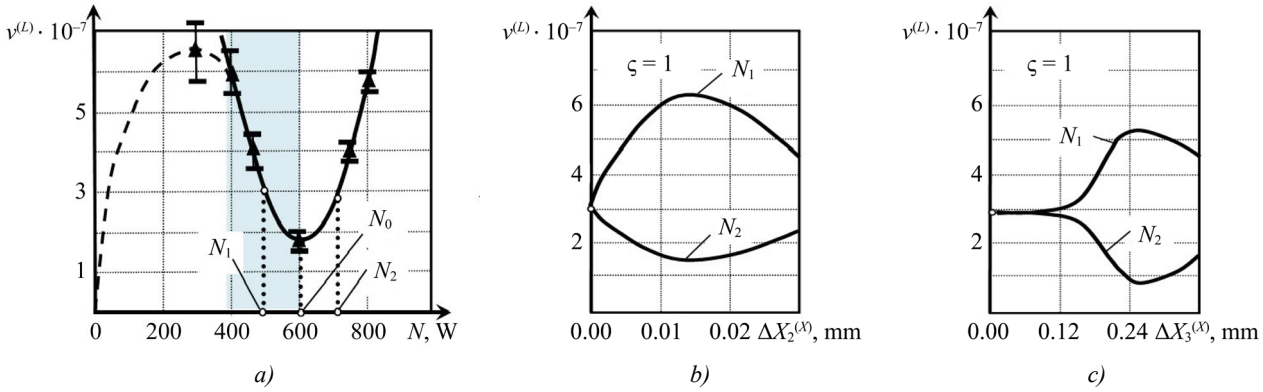

Fig. 6. Example of change in $v^{(L)}$ for cutting velocities of 1 m/s and 1.4 m/s (N_1 and N_2, respectively): *a* — trajectory $v^{(L)}$ without additional vibrations; *b* — in the direction X_2; *c* — in the direction X_3

Since vibration-free cutting is considered, then $V_p = const$. The forces on the flank are estimated by extrapolating the forces to zero cutting thickness. Dependence $v^{(L)}(N)$ (Fig. 6 *a*) has three distinct sections: in two, the power increases (clear zone), and in one, it decreases (shaded zone). Power N is estimated at a stage where wear does not exceed w = 0.2 mm. The black triangles represent experimental points, each obtained by determining the mathematical expectation from the experiments. Note that at least five experiments were conducted for each point. The well-known relationship 1 kg·m/s = 9.81 W was used to determine the power in watts.

Experimental data on the USV impact on cutter wear are visualized in Figure 7.

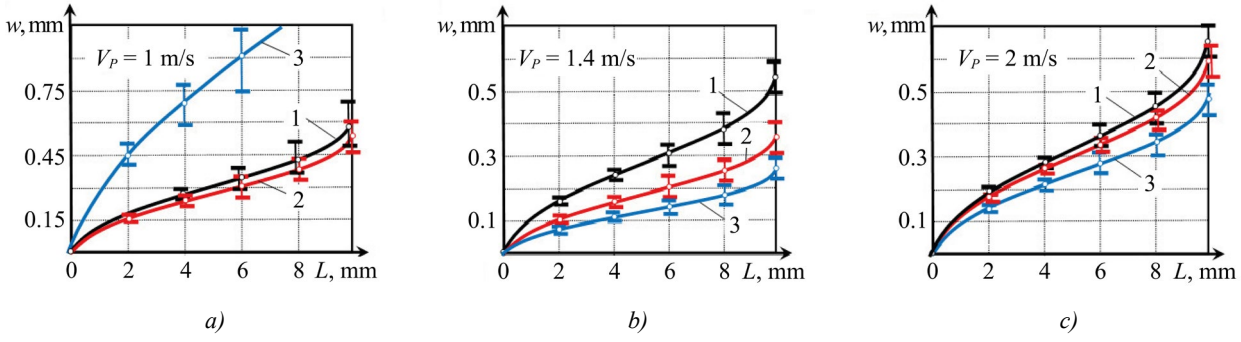

Fig. 7. Dependence of tool life on amplitude of vibrational displacements in the feed direction: *a* — at a cutting velocity of 1 m/s; *b* — at a cutting velocity of 1.4 m/s; *c* — in the tangential direction at a cutting velocity of 2 m/s.

Here, 1 — $\Delta X_i^{(X)} = 0$; 2 — $\Delta X_i^{(X)} = 5$ μm; 3 — $\Delta X_i^{(X)} = 10$ μm, i = 2, 3

The change in wear along the cutting path is the path of the tool tip across the workpiece during each revolution of its circumference. For each point of the wear characteristics, their mathematical expectations and variances relative to the mathematical expectations are shown (represented by vertical segments). In Figure 7, value of *w* at each point corresponds to at least five experiments.

Discussion. Modeling has revealed that the disproportionate increase in the force impulse varies depending on the clearance angle α. At small angles (large ς), a rapid increase is observed even at low amplitudes of the HFV. Figure 3 *a, c, d* demonstrates the limitation of additional cutting forces relative to zero. This is due to the nonlinear dependence of cutting forces on the clearance angle of the tool in model (7). This exponential function accounts for the physical constraint on the tool continuous movement along the workpiece. Therefore, the additional forces are strictly positive. The curves in Figure 3 *c, d* demonstrate an asymmetry in the rise and fall of the force impulse, which is also explained by the exponential dependence in (7). If additional vibrations are absent, the force value is determined by the exponential function $exp[\varsigma(\upsilon - \upsilon^*)] = 1$. Periodic movements relative to this point cause changes in the form of the additional force impulses, moving from the exponential section with a high rate of increment (front of impulse Φ_2 in Fig. 3 *c, d*) to a more gradual one (decay of impulse Φ_2 in Fig. 3 *c, d*). Small variations in the vibrations relative to this point cause variations in Φ_2, which, due to small deviations from the equilibrium point, can be considered in a linear approximation. Then the relationship between the vibrations and the forces remains linear, and the change in the additional forces is close to a harmonic form (Fig. 3 *b*).

As the amplitude increases, nonlinear properties of the force vibrations impact on the tool flank become apparent. Nonlinear interactions cause a displacement in the period-integrated vibrations Φ_2, as shown by the dotted lines in Figure 3 *b, c, d*. The greater the vibration amplitude, the more pronounced the constant component of the forces becomes, shifting the system equilibrium point (for the case in Fig. 3 *b* — 8 kgf, Fig. 3 *c* — 22 kgf, Fig. 3 *d* — 50 kgf). Furthermore, with an increase in the vibrational amplitude, the force surges become closer in shape to delta functions, which, taking into account the impact of forces on the current value of the power of irreversible energy transformations, causes surges in heat production and increases tool wear.

Let us note two effects when increasing the amplitude of the simulated HFV.

First, the vibrations create a cyclically stressed state in the cutting zone, redistributing the constant and cyclic forces. This leads to a decrease in the effective values of $\widehat{\rho}$, and therefore, of $\widehat{F}_0$. The elastic deformations in the region adjacent to the chip formation zone depend on this force. Elastic recovery is observed in the flank contact region. This results in the generation of forces $k_\Phi \widehat{F}_0$, whose magnitude depends on $\widehat{\rho}$.

Secondly, variation of the HFV amplitude corresponds to changes in the values of additional forces Φ_3 in the cutting direction. The force graphs are presented for various tool flank gradient ς taking into account changes in the current vibrational velocities, which essentially determines the degree of approach of the tool surface to the workpiece or, for example, the degree of its wear. As the HFV amplitude increases, the tool flank approaches the workpiece, resulting in an increase in Φ_3 (Fig. 4 *b, c, d*). However, at $\varsigma = 1$, the effect of force minimization is visible from $\Phi_3 = 42$ kgf to $\Phi_3 = 30$ kgf with increasing amplitude $\Delta X_2^{(X)}$ (Fig. 4 *b*). According to (18*b*), this indicates the existence of such amplitudes of the HFV at which power $N(t)$ in the cutting zone is minimized. This effect at $\varsigma = 5$ is weakly expressed and shifted to the left, towards the effect of small amplitudes of the HFV. In this case, a small change in force is noticeable from $\Phi_3 = 19$ kgf to $\Phi_3 = 17$ kgf (Fig. 4 *c*). At $\varsigma = 7$, this effect disappears (Fig. 4 *d*), and Φ_3 grows following the HFV amplitude to $\Phi_3 = 103$ kgf. The increment of forces $\Delta\Phi_3$ is proportional to each new value of the disturbance amplitude (Fig. 4 *d*).

Thus, as wear increases, the optimal value of the HFV amplitude, which is capable of minimizing the value of additional cutting forces on the tool flank, and, consequently, the power of irreversible energy transformations in the cutting zone, decreases.

The study allowed us to determine and visualize the amplitudes of the HFV at which the PIET takes a minimum value, and this minimum depends on parameter ς, that is, on the degree of wear of the plate. Thus, when the HFV system is disturbed in the direction V_2 for $\varsigma = 1$, the optimal amplitude will be $\Delta X_2^{(X)} = 0.025$ mm. At this value, the power released in the cutting zone is minimized (Fig 5 *a*). At $\varsigma = 5$, the optimum shifts in the direction of the arrow on the graphs. The minimum of power trajectory 2 occurs at $\Delta X_2^{(X)} \approx 0.01$ mm, and then degenerates at $\varsigma = 7$. Further, even small additional vibrations correspond to an increase in the PIET. The effects noted above are neutralized if the HFV frequency exceeds the cutoff frequency of the dynamic subsystem of the cutting process, which is determined by parameter $T^{(0)}$.

The described effects are leveled by vibrations $\Delta V_3^{(X)} sin(\Omega_0 t)$ in the direction V_3, due to which the tool deviates from the direction A — B (Fig. 5 *b*). This appears as a projection determined by the ratio V_2/V_3 (Fig. 2 *b*). Here, to the right of the dotted line ($V_3 \langle \Delta X_3 \Omega_0$), a break in contact between the tool and the cutting zone is observed. This creates a cyclically stressed state, which is caused by the periodic interruption of cutting. Therefore, the effective forces and the PIET are reduced almost by half for the trajectory at ς = 1 from N = 300 W to N = 144 W, and at ς = 5 — from N = 320 W to N = 210 W. Furthermore, at low speeds, the tool and workpiece rear faces come closer together. This creates additional forces acting on the flank. This results in an effect similar to the impact of circulatory forces, which form circular tool tip trajectories.

The paper examines in detail examples of change of $v^{(L)}$ depending on the amplitude for two velocities (V_P = 1 m/s, V_P = 1.4 m/s) and the corresponding PIET (N_1, N_2) (Fig. 6 *b*, *c*). Point N_0 = 600 W corresponds to velocity $V_P^{(0)}$ = 1.2 m/s at which $v^{(L)}$ is minimal without additional vibrations. Point N_0 = 600 W lies in the velocity range of 0.7–3 m/s. It corresponds to the optimal cutting temperature. The efficiency of the vibration impact depends on V_P, the direction of vibrations, and the entire dynamic cutting system, including the workpiece. The range in which these effects are detected is limited to frequencies of 15–20 kHz.

The contradictory effect of USV in the direction V_2 for velocities V_P = 1 m/s и V_P = 1.4 m/s Fig. 7 *a, b*) is noticeable for the same cutting path. Figure 7 *a* shows a case of an extremely insignificant decrease in the maximum value of tool wear on the flank. With the introduction of USV $\Delta X_2^{(X)}$ = 5 μm, the reduction in this indicator is limited to 0.075 mm and decreases from w = 0.575 mm (curve 1) to w = 0.5 mm (curve 2). Doubling the USV amplitude ($\Delta X_2^{(X)}$ = 10 μm, Fig. 7 *a*) leads to intensification of wear, and its maximum value increases to w = 1.05 mm (curve 3).

Here, starting from a certain amplitude, an increase in the USV intensifies the cutting force surges along the flank edge $\Phi_2(t)$. Consequently, according to (18), the energy released in this region increases, and tool wear intensifies. A similar effect was observed in numerical experiments for $\Phi_2(t)$ (Fig. 3 *b*, *c*, *d*).

Thus, in the case of introducing USV in the feed direction, the vibration efficiency in reducing tool wear depends fundamentally on the cutting velocity. Value of V_p may initially be close to the optimal value of the PIET N_0 (Fig. 6 *a*), its small variations in the cutting zone will increase heat generation and, accordingly, wear. With the introduction of USV, the minimum wear intensity shifts towards increasing V_p (Fig. 7 *b*), and the maximum wear value decreases from w = 0.55 mm (curve 1) to w = 0.35 mm (curve 2) when introducing USV with an amplitude of $\Delta X_2^{(X)}$ = 5 μm and to w = 0.26 mm (curve 3) with an amplitude of $\Delta X_2^{(X)}$ = 10 μm . This is due to a decrease in the cyclic components of the cutting forces.

The data in Figure 7 *c* suggest that at V_P = 2 m/s the tool wear rate in the direction of cutting speed is virtually independent of USV. This is due to the limited ability to vary the USV amplitude during the experiment. Under our conditions, the achievable amplitude of vibrational displacements does not exceed 10–15 μm, and at high cutting speeds, the effect of USV on wear rate will be less due to the small relative variations in vibrational velocity to cutting velocity.

Setting low cutting speeds is appropriate for certain types of machining. For example, when dealing with heat-resistant steels, the introduction of USV significantly minimizes tool wear. Therefore, to effectively utilize vibration disturbances, it is required to consider the USV amplitude under the cutting process. To select the optimal ratio between the USV amplitude and the velocity of the tool vibrational displacements, an analysis of its motion is essential.

In Figure 7 *c*, the cutting velocity value is in the zone of small change in the PIET, that is, to the left of the dotted line, as shown in Figure 5 *b*. A decrease in the maximum wear value in Figure 7 *c* from w = 0.65 mm (curve 1) to w = 0.6 mm (curve 2) is achieved at $\Delta X_3^{(X)}$ = 5 μm. Amplitude $\Delta X_3^{(X)}$ = 10 μm allows wear to be reduced to w = 0.48 mm.

Thus, numerical modeling and experiments have shown that vibrations along axis X_2 shift the optimum velocity V_P, at which wear intensity is minimized, toward increasing cutting velocity (Fig. 6 *b*, *c*). Note that for case N_1 (Fig. 6 *b*), velocity V_P is lower than the optimum cutting velocity $V_P^{(0)}$ = 1.2 m/s without vibrations. In this case, with increasing amplitude $\Delta X_2^{(X)}$ at velocity V_P, additional vibrations, as a rule, increase wear intensity. For case N_2 $V_P \rangle V_P^{(0)}$ and as the amplitude of additional vibrations increases, an extremum is observed at which wear intensity is minimized.

The overall pattern of wear rate changes depending on vibration parameters, obtained through numerical modeling, qualitatively matches the experimental results of studying the impact of USV on wear (Fig. 7). As the amplitude increases, the optimum depends not only on the process conditions but also on the initial tool geometry, such as its clearance angle. The optimum shifts as wear progresses. At a certain point, the extremum levels out, and then the introduction of additional vibrations will not increase wear resistance under any process parameters.

When additional vibrations are excited in the direction of the cutting velocity, the situation changes. Here, the extreme amplitude of the vibrational velocity is observed only in the low-speed range. With USV, the existence of an optimal amplitude in the direction of the cutting velocity is limited to a cutting velocity of 0.3–0.5 m/s.

The reduction in wear rate depends on all the basic parameters of the DCS. Here, first of all, the elements of the stiffness matrices and the generalized masses should be mentioned. Furthermore, it is important to consider the dynamic coupling parameters, whose effective values themselves depend on the vibrations. Additional vibrations from the ultrasonic acoustic system (for example, in the feed direction) change not only the spatial orientation but also the amplitude due to the reaction from the cutting process. The resulting phase shifts between vibrations in different directions depend on the amplitude. They are caused by the specific interactions between vibrations on forces and forces — on deformations. Therefore, for example, it is impossible to orient additional vibrations in the direction of the projected cutting velocity (direction *A* — *B* in Figure 2).

Thus, even small-amplitude HFV always cause periodic changes in the approach between the tool flank and workpiece. This explains the first trend — an increase in wear rate with increasing amplitude. The second trend is caused by the development of a cyclically stressed state in the primary and secondary deformation zones. As a result, the forces and the PIET decrease in the contact zone between the flank and workpiece. These two opposing trends determine the dependence of wear rate on vibrational amplitude. It should also be noted that the optimal amplitude in all cases in a given system changes as wear progresses, as this process transforms the geometry of the tool flank.

Conclusion. The findings of the research presented in this article differ from those of published studies on the impact of vibration on tool wear. The author shows changes in cutting tool wear as a function of high-frequency vibrations from a new perspective — through the relationship between the power of irreversible energy transformations at a specific location, namely, the contact area between the workpiece and the tool flank. Previously, wear was considered in the literature on the scale of the entire cutting process.

The following tasks were accomplished in the course of the work.

1. It is shown that HFV affect tool wear rate with varying efficiency. The result depends on the tool geometry, its current wear, cutting velocity, and the parameters of the dynamic model of the cutting system.

2. The regularities linking the HFV with the tool wear rate are analytically validated.

3. The use of a numerical model of DCS as a basis for hybrid systems of dynamic wear monitoring is described.

4. Experimental results are presented that verify the contradictory effect of increasing the USV amplitude for different velocity ranges.

The proposed approach allows us to explain changes in the system properties in the low- and mid-frequency regions depending on the amplitude of the HFV. HFV introduced into the cutting zone can be considered as a control factor for:

– tool wear;

– dynamic properties of the cutting system.

The adequacy of the modeling results is limited by the zone of tool wear rate, in which the effect of random processes on the dynamics of the system increases and, accordingly, the assessment of the accuracy of the model is significantly reduced.

Conditions where the amplitude of vibrational displacements exceeds 10–15 μm require additional studies. Furthermore, it is necessary to elucidate the intrasystem physical processes of molecular-mechanical wear, including the physics of interactions as a whole. A promising direction for the developed models is their integration into tool wear diagnostic systems based on hybrid machine learning architectures. This approach will enable more accurate prediction of changes under the condition of cutting tools when modeling DSR.

References

1. Shaojian Zhang, Sandy Suet To, Guoqing Zhang, Zhiwei Zhu. A Review of Machine-Tool Vibration and Its Influence upon Surface Generation in Ultra-Precision Machining. *International Journal of Machine Tools and Manufacture*. 2015;91:34–42. https://doi.org/10.1016/j.ijmachtools.2015.01.005

2. Aman Ullah, Tzu-Chi Chan, Shinn-Liang Chang. Current Trends in Vibration Control and Computational Optimization for CNC Machine Tools: A Comprehensive Review. *The International Journal of Advanced Manufacturing Technology.* 2025;139(11):5409–5444. https://doi.org/10.1007/s00170-025-16238-8

3. Kudinov VA. *Machine Tool Dynamics*. Moscow: Mashinostroenie; 1967. 359 p. (In Russ.)

4. Tobias SA, Fishwick W. Theory of Regenerative Machine Tool Chatter. *The Engineer*. 1958;205(7):199–203. URL: https://vibraction.fr/images/stories/Documents/1erePresentationLobesTobias.pdf (accessed: 10.11.2025).

5. Vela-Martínez L, Jáuregui-Correa J-C, González-Brambila O, Herrera-Ruiz G, Lozano-Guzmán A. Modeling of Machining Processes for Predictive Analysis of Self-excited Vibrations. *Ingeniería Mecanica, Tecnología y Desarrollo*.2008;3(2):1–9. URL: https://scielo.org.mx/pdf/imtd/v3n1/v3n1a2.pdf (accessed: 10.11.2025).

6. Zakovorotny VL, Lukyanov AD, Gubanova AA, Hristoforova VV. Bifurcation of Stationary Manifolds Formed in the Neighborhood of the Equilibrium in a Dynamic System of Cutting. *Journal of Sound and Vibration*. 2016;368:174–190. https://doi.org/10.1016/j.jsv.2016.01.020

7. Caixu Yue, Haining Gao, Xianli Liu, Steven Y Liang, Lihui Wang. A Review of Chatter Vibration Research in Milling. *Chinese Journal of Aeronautics.* 2019;32(2):215–242. https://doi.org/10.1016/j.cja.2018.11.007

8. Gouskov AM, Guskov MA, Lorong Ph, Panovko G. Influence of Flank Face on the Condition of Chatter Self-excitation during Turning. *International Journal of Machining and Machinability of Materials.* 2017;19:17–40. https://doi.org/10.1504/IJMMM.2017.081186

9. Zakovorotny V. Bifurcations in the Dynamic System of the Mechanic Processing in Metal-Cutting Tools. *WSEAS Transactions on Applied and Theoretical Mechanics*. 2015;10:102–116. URL: https://www.wseas.org/multimedia/journals/mechanics/2015/a225811-099.pdf (accessed: 10.11.2025).

10. Zakovorotny VL, Gvindjilia VE. *Fundamentals of System-Synergetic Analysis and Synthesis of Process Control on Metal-Cutting Machines*. Saint Petersburg: Lan'; 2025. 436 p. (In Russ.)

11. Altintas Y, Eynian M, Onozuka H. Chatter stability of machining operations. *Journal of Manufacturing Science and Engineering.* 2020;142(11):110801. https://doi.org/10.1115/1.4047391

12. Sujuan Wang, Tao Zhang, Wenping Deng, Zhanwen Sun, Sandy To. Analytical Modeling and Prediction of Cutting Forces in Orthogonal Turning: A Review. *The International Journal of Advanced Manufacturing Technology.* 2022;119(3):1407–1434. https://doi.org/10.1007/s00170-021-08114-y

13. Rusinek R, Wiercigroch M, Wahi P. Modelling of Frictional Chatter in Metal Cutting. *International Journal of Mechanical Sciences.* 2014;89:167–176. https://doi.org/10.1016/j.ijmecsci.2014.08.020

14. An-Hong Tian, Cheng-Biao Fu, Xiao-Yi Su, Her-Terng Yau. Lathe Tool Chatter Vibration Diagnostic Using General Regression Neural Network Based on Chua's Circuit and Fractional-order Lorenz Master/Slave Chaotic System. *Journal of Low Frequency Noise, Vibration and Active Control.* 2019;38(3/4):953–966. https://doi.org/10.1177/1461348418815414

15. Katiyar S, Muskan J, Narain RP, Singh S, Shrivastava Y. A Short Review on Investigation and Suppression of Tool Chatter in Turning Operation. *Materials Today: Proceedings.* 2022;51(1):1206–1210. https://doi.org/10.1016/j.matpr.2021.07.208

16. An Wang, Baiyuan Zhou, Wuyin Jin. Dynamics of the Regenerative Turning Chatter with Little Mass Eccentricity. *International Journal of Non-Linear Mechanics.* 2024;166:104851. https://doi.org/10.1016/j.ijnonlinmec.2024.104851

17. Forestier F, Gagnol V, Ray P, Paris H. Model-Based Cutting Prediction for a Self-vibratory Drilling Head-Spindle System. *International Journal of Machine Tools and Manufacture.* 2012;52(1):59–68. https://doi.org/10.1016/j.ijmachtools.2011.09.001

18. Pengfei Zhang, Dongbo Hong, Giovanni Totis, Federico Scalzo, Zengbin Yin, Liming Shu L, et al. Systematic Review of Cutting Force Measuring Systems in Machining: Principles, Design, Filtering Techniques and Applications. *International Journal of Machine Tools and Manufacture*. 2025;210:104308. https://doi.org/10.1016/j.ijmachtools.2025.104308

19. Xue-Bin Qin, Min Wan, Wei-Hong Zhang, Yun Yang. Chatter Suppression with Productivity Improvement by Scheduling a C^3 Continuous Feedrate to Match Spindle Speed Variation. *Mechanical Systems and Signal Processing*. 2023;188:110021. https://doi.org/10.1016/j.ymssp.2022.110021

20. Zakovorotny VL, Lukyanov AD. The Problems of Control of the Evolution of the Dynamic System Interacting with the Medium. *International Journal of Mechanical Engineering and Automation.* 2014;1(5):271–285. URL: https://www.researchgate.net/publication/293636021_The_Problems_of_Control_of_the_Evolution_of_the_Dynamic_System_Interacting_with_the_Medium (accessed: 10.11.2025).

21. Sergiev AP, Vladimirov AA, Makarov AV, Shvachkin EG. Physical Fundamentals of the Vibratory Cutting Process in Turning. *Bulletin of Belgorod State Technological University named after V.G. Shukhov.* 2017;(3):94–102. (In Russ.) https://doi.org/10.12737/24626

22. Ghorbani S, Kopilov VV, Polushin NI, Rogov VA. Experimental and Analytical Research on Relationship between Tool Life and Vibration in Cutting Process. *Archives of Civil and Mechanical Engineering.* 2018;18(3):844–862. https://doi.org/10.1016/j.acme.2018.01.007

23. Canbin Zhang, Xiaoliang Liang, Chi Fai Cheung, Chunjin Wang, Benjamin Bulla. Theoretical and Experimental Investigation of Ultrasonic Cutting Kinematics and Its Effect on Chip Formation and Surface Generation in High-Frequency Ultrasonic Vibration-assisted Diamond Cutting. *Journal of Materials Research and Technology.* 2024;30:5662–5676. https://doi.org/10.1016/j.jmrt.2024.04.266

24. Qingliao He, Yun He, Xin Wang, Biao Zhao, Wenfeng Din. Effects of Longitudinal-Torsional Ultrasonic Vibration on the Tool Wear Characteristics and Performance in Side Milling of GH4169 Superalloy. *The International Journal of Advanced Manufacturing Technology.* 2025;140:3171–3184. https://doi.org/10.1007/s00170-025-16490-y

25. Renke Kang, Shenghao Chao, Jiansong Sun, Jinchuan Luan, Zhigang Dong, Yidan Wang. Study on the Cutting Performance of Ultrasonic-assisted Turning for Cast Superalloy K4169. *The International Journal of Advanced Manufacturing Technology.* 2025;137:1089–1102. https://doi.org/10.1007/s00170-025-15216-4

26. Zhaojie Yuan, Daohui Xiang, Peicheng Peng, Zhiqiang Zhang, Binghao Li, Mingyang Ma, et al. A Comprehensive Review of Advances in Ultrasonic Vibration Machining on SiCp/Al Composites. *Journal of Materials Research and Technology.* 2023;24:6665–6698. https://doi.org/10.1016/j.jmrt.2023.04.245

27. Astashev VK, Andrianov NA, Krupenin VL. On Autoresonant Ultrasonic Cutting Materials. *Bulletin of Scientific and Technical Development.* 2017;(1(113)):3–16.

28. Agapov SI, Kirakosyan KA, Arzhukhanov RI, Novikova LA. The Use of Ultrasonic Vibrations in Turning. *Izvestia VSTU.* 2022;267(8):7–9. https://doi.org/10.35211/1990-5297-2022-8-267-7-9

29. Ghule G, Sanap S, Chinchanikar S. Ultrasonic Vibration-Assisted Hard Turning of AISI 52100 Steel: Comparative Evaluation and Modeling Using Dimensional Analysis. *Metal Working and Material Science.* 2023;25(4):136–150. https://doi.org/10.17212/1994-6309-2023-25.4-136-150

30. Agapov SI, Tkachenko IG. Determining the Optimal Amplitudes and Directions of Ultrasound Vibrations in Cutting Small-Module Gears. *Russian Engineering Research.* 2010;30(2):141–143. https://doi.org/10.3103/S1068798X10020103

31. Astakhov VP, Outeiro J. Importance of Temperature in Metal Cutting and Its Proper Measurement/Modeling. In book: Davim J. (ed) *Measurement in Machining and Tribology.* Cham: Springer; 2018. P. 1–47. URL: https://link.springer.com/chapter/10.1007/978-3-030-03822-9_1 (accessed: 07.12.2025).

32. Astakhov VP, Xinran Xiao. The Principle of Minimum Strain Energy to Fracture of the Work Material and Its Application in Modern Cutting Technologies. In book: *Metal Cutting Technologies. Progress and Current Trends.* Munich: De Gruyter Oldenbourg; 2016. P. 1–35. URL: https://clck.ru/3SWbzm (accessed: 07.12.2025).

33. Lyubimyi N.S., Chetverikov B.S., Gerasimov M.D., Bytsenko M.V., Pol'shin A.A., Mal'tsev A.K. Experimental Study and Modeling of Thermal Response in Turning a 3.5 mm Thick Shell of Metal Composite System. *Advanced Engineering Research (Rostov-on-Don).* 2026;26(1):2250. https://doi.org/10.23947/2687-1653-2026-26-1-2250

34. Tavstyuk AA, Lyutov AG, Kourou GN. Application of Specific Energy Parameters in Optimization and Control of the Cutting Process. *STIN.* 2014;(2):29–34. (In Russ).

35. Yanov ES, Antonychev SV, Antsev AV, Vorotilin MS, Minakov EI. Studying Methods for Controlling the Condition of Milling Machines Based on the Analysis of Vibration Characteristics. *University Proceedings. Volga Region. Engineering Sciences.* 2024;(3(71)):157–166. https://doi.org/10.21685/2072-3059-2024-3-14

36. Yuqing Zhou, Wei Xue. Review of Tool Condition Monitoring Methods in Milling Processes. *International Journal of Advanced Manufacturing Technology.* 2018;96:2509–2523. https://doi.org/10.1007/s00170-018-1768-5

37. Xuchen Hou, Wei Xia, Xianli Liu, Caixu Yue, Xiao Zhang, Dingfeng Yan. Research on Milling Cutter Wear Monitoring Based on Self-learning Feature Boundary Model. *The International Journal of Advanced Manufacturing Technology.* 2024;135(3):1789–1807. https://doi.org/10.1007/s00170-024-14532-5

38. Kozochkin MP, Sabirov FS, Seleznev AE. Vibroacoustic Monitoring of Cutting Edge Machining of Hardened Steel. *Vestnik MSTU "Stankin".* 2018;(1(44)):23–30.

39. Zakovorotny VL, Gvindzhiliya VE. System-Synergetic Analysis and Synthesis of a Controlled Cutting Process. *Science Intensive Technologies in Mechanical Engineering.* 2024;(9):3–13. https://doi.org/10.30987/2223-4608-2024-3-13

40. Zakovorotny VL, Gvindzhiliya VE. Influence of the Tool Vibration on the Part Surface in Longitudinal Turning. *Proceedings of Higher Educational Institutions. Machine Building.* 2024;(9(774)):52–71.

41. Zakovorotny VL, Gvindzhiliya VE. Influence of Spindle Wobble in a Lathe on the Tool's Deformational-Displacement Trajectory. *Russian Engineering Research*. 2018;38(8):623–631. https://doi.org/10.3103/S1068798X1808018X

42. Blekhman I, Blekhman LI, Vaisberg LA, Vasilkov VB. Energy and Frequency Ripple in Devices with Inertial Excitation of Oscillations. *Philosophical Transactions. Series A. Mathematical, Physical and Engineering Sciences.* 2021;379(2198):20200233. https://doi.org/10.1098/rsta.2020.0233

43. Bogolyubov NN, Mitropolsky YuA. *Asymptotic Methods in the Theory of Nonlinear Oscillations*. Moscow: Nauka; 1974. 503 p. (In Russ).

44. Zorev NN. *Questions of the Mechanics of Metal Cutting Processes*. Moscow: Mashgiz; 1956. 368 p. (In Russ).

45. Zakovorotny VL, Pham Dinh Tung, Chiem Nguyen Xuan, Ryzhkin MN. Dynamic Coupling Modeling Formed by Turning in Cutting Dynamics Problems (Velocity Coupling). *Vestnik of Don State Technical University.* 2011;11(2):137–146. URL: https://www.vestnik-donstu.ru/jour/article/view/702/701 (accessed: 07.12.2025).

46. Zakovorotny VL, Pham Dinh Tung, Chiem Nguyen Xuan, Ryzhkin MN. Dynamic Coupling Modeling Formed by Turning in Cutting Dynamics Problems (Positional Coupling). *Vestnik of Don State Technical University.* 2011;11(3):301–311. URL: https://www.vestnik-donstu.ru/jour/article/view/725/724 (accessed: 07.12.2025).

47. Zakovorotny VL, Gvindjiliya VE. The Study of Vibration Disturbance Mapping in the Geometry of the Surface Formed by Turning. *Metal Working and Material Science.* 2024;26(2):107–126. https://doi.org/10.17212/1994-6309-2024-26.2-107-126

About the Author:

Valery Y. Gvindjiliya, Cand.Sci. (Eng.), Senior Lecturer of the Automation of Production Processes Department, Don State Technical University (1, Gagarin Sq., Rostov-on-Don, 344003, Russian Federation), SPIN-code, ORCID, ScopusID, ResearcherID, vvgvindjiliya@donstu.ru

Conflict of Interest Statement: **the author declares no conflict of interest.**

The author has read and approved the final manuscript.

Об авторе:

Валерия Енвериевна Гвинджилия, кандидат технических наук, старший преподаватель кафедры «Автоматизация производственных процессов» Донского государственного технического университета (344003, Российская Федерация, г. Ростов-на-Дону, пл. Гагарина, 1), SPIN-код, ORCID, ScopusID, ResearcherID, vvgvindjiliya@donstu.ru

Конфликт интересов: **автор заявляет об отсутствии конфликта интересов.**

Автор прочитал и одобрил окончательный вариант рукописи.

Received / **Поступила в редакцию** 08.12.2025
Reviewed / Поступила после рецензирования 12.01.2026
Accepted / **Принята к публикации** 26.01.2026